Journal of Catalysis 280 (2011) 196–205

Contents lists available at ScienceDirect

Journal of Catalysis

journal homepage: www.elsevier.com/locate/jcat

Structure–deactivation relationship for ZSM-5 catalysts governed by framework defects

Katia Barbera [a], Francesca Bonino [a], Silvia Bordiga [a], Ton V.W. Janssens [b], Pablo Beato [b,*]

[a] Department of Inorganic, Physical and Materials Chemistry, INSTM Centro di Riferimento and NIS Centre of Excellence, Universita' di Torino, Via Quarello 11A, 10125 Torino, Italy
[b] Haldor Topsøe A/S, Nymøllevej 55, DK-2800 Lyngby, Denmark

ARTICLE INFO

Article history:
Received 25 November 2010
Revised 16 March 2011
Accepted 20 March 2011
Available online 23 April 2011

Keywords:
Zeolites
H-ZSM-5
Deactivation
Defects
Methanol to hydrocarbons

ABSTRACT

Zeolites are well known catalysts for the conversion of methanol to hydrocarbons. By adjusting the synthesis procedure, the activity and deactivation of the ZSM-5 zeolite in the conversion of methanol to gasoline can be varied significantly. We found that internal framework defects are crucial for the deactivation behavior of the ZSM-5 catalysts. Adsorption of pyridine and 2,4,6-collidine shows that the infrared band at 3745 cm^{-1} can be assigned to isolated silanol groups on the external surface and the bands at 3726 and 3700 cm^{-1} to silanol groups inside the zeolite crystals. While the activity is related to the acid site density, the deactivation rate correlates with the measured intensity ratio of the IR bands for internal silanols at 3726 cm^{-1} and for external silanol groups at 3745 cm^{-1} (I_{3726}/I_{3745}). The activity and deactivation, therefore, depend on a different physical property, which means that they can be varied independently.

© 2011 Elsevier Inc. All rights reserved.

1. Introduction

The conversion of methanol to hydrocarbons (MTH) over acidic nanoporous materials is a well known reaction [1–3]. In the TIGAS process, the synthesis of methanol and DME is integrated with the hydrocarbon formation, resulting in a truly synthesis gas-to-gasoline process [4]. ZSM-5 and SAPO-34 are the archetype catalysts for the conversion of methanol to hydrocarbons and are still regarded as the most effective catalysts [5,6].

The relatively slow deactivation rate of ZSM-5, which makes this zeolite the preferred catalyst for the conversion of methanol to hydrocarbons, is attributed to its characteristic three dimensional micropore system. The size of the 10-ring micropores (5.1–5.6 Å) prevents the formation of large condensed polyaromatic compounds (coke) inside the channels of the zeolite [7–11], and the three dimensional channel structure ensures the accessibility of the acid sites. Therefore, coking of ZSM-5 is often described as an external surface phenomenon, eventually leading to the blockage of the pore entrances [12]. The presence of internal coke during methanol conversion over ZSM-5 has been reported as well [9], but it is difficult to distinguish coke precursors from the polymethylated benzenes, which are the active species in the hydrocarbon pool mechanism [13–15]. It is even conceivable that polymethylated benzenes can act as both active intermediates and coke precursors, depending on their local environment inside the microporous framework of ZSM-5 [16].

The activity of a ZSM-5 catalyst, or any other acid material, for the conversion of methanol is determined by the nature, the amount, and the accessibility of its acid sites. In general, the activity increases with increasing acid site density for similar materials, while different materials with the same acid site density show different activities. In addition, it is well known that the activity of solid catalysts also can be influenced by structural defects [17–19], such as steps, kinks, or dislocations. For example, the active sites for the rearrangement of cyclohexanone oxime to ε-caprolactam over an MFI-type silicalite, which has the same structure as ZSM-5 but does not have Brønsted acid sites, are the silanol defects in the silicalite structure [20–22]. This clearly illustrates that structural defects in zeolites can be important for the catalytic activity.

Silanol defects can also play a role for coke formation in a ZSM-5 catalyst. In a study by Thibault-Starzyk et al. [23], a direct correlation is made between the formation of coke and the presence of silanol defects in the isomerization of ortho-xylene over H-ZSM-5. From a 2D correlation analysis of in situ IR spectroscopy data, it was found that coke deposits were mainly located on non-acidic silanol groups inside the micropore system. This constitutes an example that silanol groups also are an important factor for coke formation. Since coke formation is a major route for catalyst deactivation, this strongly suggests that the silanol groups also affect the deactivation behavior of zeolite catalysts. Nevertheless, the role of these silanols and related defects for the conversion of hydrocarbons is not very well understood and is often given a

* Corresponding author. Fax: +45 45272999.
E-mail address: pabb@topsoe.dk (P. Beato).

0021-9517/$ - see front matter © 2011 Elsevier Inc. All rights reserved.
doi:10.1016/j.jcat.2011.03.016

minor importance in many studies on deactivation via coking [7–12,24,25].

To investigate how the activity and, in particular, the deactivation relate to the micro-structural properties of the zeolite, we present measured activities and deactivation rates in the conversion of methanol to hydrocarbons of over a large variety of different ZSM-5 catalysts. These different ZSM-5 catalysts were synthesized using a number of different synthesis methods and treatments. The activities and deactivation rates are extracted from measurements of the methanol conversion with time on stream, according to a recently developed model [26]. For a selection of samples, these properties are related to the acid site density and silanol group density of the ZSM-5 catalysts. The silanol groups and related structural defects are effectively characterized by IR spectroscopy [27–33], and a clear correlation between the features in the IR spectrum related to the silanol groups and the measured catalyst deactivation can be established.

2. Materials and methods

2.1. Sample preparation

A wide range of ZSM-5 zeolites was synthesized using different synthesis procedures and post-treatments to produce materials with variations in particle sizes, acidity, metal doping, and desilication with NaOH [34–39]. In this article, we concentrate on two series of non-treated, pure ZSM-5 materials, one with a particle size of 100 nm and a second with a particle size of 300 nm, with varying Si/Al ratio, or acid site density, as listed in Table 1, and on some desilicated ZSM-5 materials.

The synthesis of the series of pure ZSM-5 zeolites mentioned above is based on a procedure commonly known as the "clear solution synthesis" developed by Schoeman et al. [40,41] which results in a crystalline material with a very narrow particle size distribution. The series of materials with 100 nm particles, with Si/Al ratios between 80 and 160, were prepared as follows (example for Si/Al = 150): 238.74 g of 40 wt.% tetrapropylammonium hydroxide (TPAOH) solution in water (AppliChem GmbH) and 139.24 g water were mixed to obtain a clear solution, which was cooled down in an ice-bath. A 3.52 g of aluminum nitrate nonahydrate (Riedel-de Haën) was dissolved in the cooled solution followed by drop wise addition of 293.49 g tetraethylorthosilicate (TEOS, Aldrich). The mixture was allowed to reach room temperature over night, to ensure a homogeneous hydrolysis and co-condensation of the reactants. The ethanol formed was evaporated under reduced pressure and a temperature not exceeding 318 K. The resulting clear gel was transferred to a Teflon® lined steel autoclave to crystallize it for 40 h at 453 K. The series with 300 nm particles, with Si/Al ratios between 80 and 180, was prepared by exactly the same procedure as described above, except that the gel was crystallized for 1 h at 453 K in a microwave oven instead of 40 h in a conventional oven. In this article, the materials are named as follows: after the letters NZ (for nano-zeolite), first the particle diameter in nanometers is given, followed by the Si/Al ratio, as determined from NH_3-TPD; for example, NZ-100/77 has a particle size of 100 nm with a Si/Al ratio of 77.

The desilicated materials discussed in this study are based on the calcined NZ-300/120 zeolite and a commercially available ZSM-5 material (Zeochem International: PZ-2/100H). The desilication procedure was as follows: The starting materials were treated with a 0.3 M NaOH solution (33 mL solution per gram catalyst material) for 30 min at 343 K, followed by cooling in an ice-bath to stop the desilication, and then washed three times with water by centrifugation. The desilicated ZSM-5 was dried over night at room temperature before further treatment. The acidic form of the desilicated zeolite was produced by two consecutive ion exchanges with a buffer solution of 1.7 M NH_4NO_3/0.94 M NH_3, using 10 mL solution per gram catalyst, at 353 K under stirring for 2 h. After each exchange, the NH_4-form of the zeolites was filtered, washed with water, and dried in air at 383 K. The final H-form of the parent zeolite and desilicated zeolite was obtained by heating the NH_4-form in air to 823 K for 3 h. The desilicated NZ-300/120 material is referred to as DZ-300/120 (for desilicated zeolite); the fresh and desilicated PZ-2/100H is referred to as PZ-ZSM-5 and DPZ-ZSM-5, respectively.

2.2. Characterization of the materials

The quality of the synthesis was checked with Inductively Coupled Plasma with Optical Emission Spectroscopy (ICP-OES) to determine the chemical composition of the materials and by X-ray powder diffraction (XRD) to verify the crystallinity of the materials. The diffraction patterns were recorded on a Philips PW1820 powder diffractometer, using Cu Kα radiation in the 2θ interval 5–80°.

The acid site density of the synthesized materials was determined by temperature programmed desorption of ammonia (NH_3-TPD). A 100 mg sample (150–300 μm sieve fraction) was dried in N_2 at 773 K for 2 h and cooled to 423 K. Ammonia is adsorbed at that temperature for about 30 min, using a mixture of 2% NH_3 in He, and purged in pure N_2 for 3 h to remove all loosely bound NH_3. Then, the temperature is increased to 1123 K with 10 K/min in a flow of approximately 50 mL/min N_2, which is bubbled through an aqueous solution of boric acid (4 w%). The total amount of NH_3 desorbed is then determined by titration of the boric acid solution with a 0.01 M solution of HCl to a pH of 4.9. For the commercial sample and its desilicated counterpart, NH_3-TPD was measured with the same temperature program as described for

Table 1
Overview of the two synthesized series of nano zeolites (NZ) and the commercial sample (PZ). Desilicated samples are labeled with a (D) as the first letter.

Sample	NH_3 capacity (mmol NH_3/g_{cat})	Si/Al (NH_3)	Si/Al (ICP)	Activity (mol_{MeOH}/g_{cat} h)	Deactivation (mg_{cat}/mol_{MeOH})
NZ-100/83	0.198	83	77	41.97	13.62
NZ-100/120	0.138	120	116	23.63	24.34
NZ-100/150	0.110	150	150	14.72	20.25
NZ-100/152	0.109	152	150	7.50	23.93
NZ-100/165	0.101	164	160	5.88	24.52
NZ-300/91	0.181	91	99	28.39	20.26
NZ-300/120	0.138	120	115	27.24	18.3
DZ-300/120	0.127	130	114	16.32	8.21
NZ-300/130	0.127	130	132	13.66	24.11
NZ-300/145	0.114	145	144	13.03	28.06
PZ-ZSM-5	0.278	50[a]	54	43.12	13.29
DPZ-ZSM-5	0.170	97[a]	19	14.39	3.62

[a] Determined by NH_3-TPD–TGA (see materials and methods).

the other samples but instead of titration with boric acid, the NH_3 desorption was followed by a gravimetric analysis. For the Si/Al ratio, only the high temperature peak (~690 K), representing the Brønsted sites, was considered.

The particle size and size distribution of the materials were checked with Scanning Electron Microscopy (SEM), using a FEI XL30 electron microscope with a field emission gun. The calcined zeolite samples were placed on aluminum stubs with double sided carbon tapes. To minimize charging, the samples were coated with a thin layer of Pt/Pd (approximately 8.6 nm in thickness).

The FTIR measurements to characterize the silanol groups in the zeolite material were performed on a Nicolet 6700 FTIR spectrometer, operating in transmission mode at 2 cm^{-1} resolution on self-supported pellets. To study the changes in hydroxyl group amount and distribution with temperature, the samples were pre-treated at 623 K and 773 K at $p \leqslant 1 \times 10^{-4}$ mbar for 1 h. The OH groups were further characterized with pyridine, 2,4,6-collidine, and CO probe molecules. Adsorption of pyridine and 2,4,6-collidine was performed by exposing the pellets to the vapor pressure of the respective compounds at room temperature. The differences in acid strength and distribution of the different OH groups were derived from the changes in IR absorption of CO probe molecules adsorbed at 100 K and a partial pressure of 70 mbar. In order to have the possibility to compare band intensities within the full set of spectra, spectra have been normalized to the overtone modes in the 1750–2100 cm^{-1} region and counterchecked by normalization to the pellet thickness. Special care has been devoted to follow the same activation procedure for all the samples.

2.3. Measurement of activity and deactivation

The catalytic activity and deactivation rate for the conversion of methanol to hydrocarbons were determined from the measured hydrocarbon yield with time on stream at constant flow, pressure, and temperature. The measurements were performed in a parallel reactor setup consisting of 10 parallel reactor channels, in which each channel is exposed to the same reaction feed gas at the same reaction conditions. Each reactor channel was filled with a 150 mg sample of the catalyst (sieve fraction 150–300 μm) and exposed to a feed of about 15% methanol in N_2 at 623 K and 15 barg, using a total flow of 307 or 350 NmL/min, which resulted in a flow between 30 and 40 NmL/min in each individual reactor channel. These conditions correspond to a WHSV of about 3 g_{MeOH}/g_{cat} h. The reactor exit gas was analyzed by sequentially connecting the individual reactor channels to a mass spectrometer (Balzers GAM 400 or Balzers ThermoStar) via a 12 ports channel selection valve. The conversion (hydrocarbon yield) in the reaction exit gas was determined by following $m/e = 32$ (methanol) and $m/e = 46$ (DME) signals with time [26]. The deactivation rate is effectively characterized by a deactivation coefficient, which is readily calculated as the ratio of the applied contact time and the catalyst lifetime to 50% conversion; the activity is found from the catalyst lifetime to 80% conversion, with a known deactivation rate [26].

3. Results

3.1. Catalyst characterization

Fig. 1 shows a typical SEM image of the synthesized ZSM-5 zeolites for the 100 nm series (left panel, Si/Al = 120) and 300 nm series (right panel, Si/Al = 120). The images show that the particles are regularly shaped and reflect the narrow size distribution. XRD confirmed that the samples are well crystallized ZSM-5 zeolites. For the 100 nm series, the Scherrer equation also yields an average crystal size between 90 and 100 nm, indicating that the particles are monocrystalline. For the 300 nm particles, the crystal sizes were too large to be determined accurately by XRD.

Fig. 2 shows a characteristic IR spectrum of a ZSM-5 zeolite in the range 3800–3000 cm^{-1}, which corresponds to the OH-stretch vibrations in the ZSM-5 zeolites. There are three relevant features for this study in this range. The first one is the band at

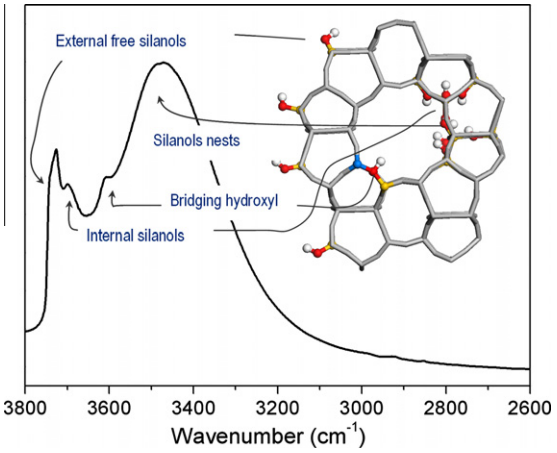

Fig. 2. Characteristic IR spectrum of an H-ZSM-5 sample activated at 623 K. A schematic representation of the different families of hydroxyl groups is reported in the characteristic cut-out of the MFI structure reported in the right side of the picture.

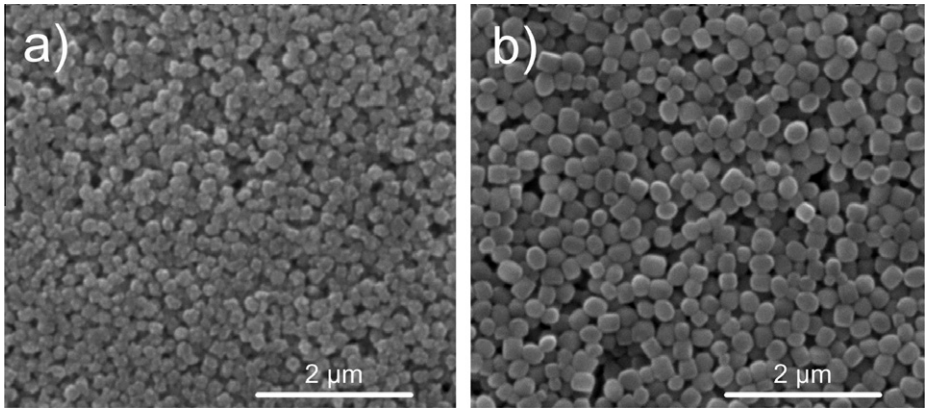

Fig. 1. Representative SEM images for the two nano-ZSM-5 series, showing the typical round shaped morphology and the extremely narrow particle size distribution. 100 nm series (a) and 300 nm series (b).

3500 cm^{-1}, which is generally ascribed to silanol nests that consist of a number of silanol groups interacting through extended hydrogen bonding. Such nests typically occur at crystal steps or extended defects [31–33]. The second feature is the well known band at 3610 cm^{-1}, corresponding to the Brønsted acid sites formed by the OH group located between a Si and Al atom in the crystal structure. The third feature is the band at 3700–3750 cm^{-1}, corresponding to more isolated silanol groups [28,29]. In fact, this band actually consists of a triplet at 3745, 3735, and 3726 cm^{-1} and a smaller and broader second one at around 3700 cm^{-1}, as a result of the existence of silanol groups in different environments. The intensity ratio of all the components, and in particular of those of the last triplet, shows some difference among the full set of samples and changes substantially in respect of the activation temperature. Below, these bands due to the silanol groups are studied in more detail.

To determine whether the different silanol groups are located inside the micropores or on the external surface, pyridine and 2,4,6-collidine (2,4,6-trimethylpyridine) were adsorbed [42–47]. Pyridine, which has a diameter of 5.7 Å, is able to enter the micropores of the ZSM-5 zeolite, while 2,4,6-collidine, with a diameter of 7.4 Å, is too large to enter these pores. Therefore, pyridine interacts with all silanol groups, but 2,4,6-collidine can only interact with sites located at the external surface [46,47]. As a consequence, if a silanol band is affected by the adsorption of pyridine, but not by 2,4,6-collidine, it is located at a site that is inaccessible for collidine, which means inside the micropores of the zeolite. Fig. 3a compares IR for NZ-100/152 (curve 1) and DZ-300/120 (curve 1-D) samples interacting with pyridine (curves 2 and 2-D, respectively) and collidine (curves 3 and 3-D, respectively) vapor pressure. As can be seen, adsorption of pyridine results in a strong reduction in all hydroxyl bands, consistent with the fact that the pyridine interacts with the hydroxyl groups both inside the micropores and on the external surface. In contrast, with adsorbed 2,4,6-collidine only the band at 3745 cm^{-1} is attenuated, while the other OH-species remain visible in the spectra. This behavior is particularly remarkable in the case of desilicated sample, whose ratio between external and internal silanols is higher. Therefore, it can be concluded that the silanol groups associated with the band at 3745 cm^{-1} are located on the outer surface and those associated with the bands at 3726 and 3700 cm^{-1} are located inside the micropores.

Fig. 3b and c show the ring vibrational modes (1670–1330 cm^{-1}) of the irreversibly adsorbed portion of pyridine and collidine molecules, i.e. the part that is not removed by evacuation at room temperature. In the case of pyridine (Fig. 3b), four bands at 1638 cm^{-1} (8a mode), 1626 cm^{-1} (8b mode), 1547 cm^{-1} (19b mode), and 1490 cm^{-1} (19a mode) are ascribed to protonated pyridine (PyH^+) [42]. The features corresponding to the ring stretching mode of hydrogen bonded to weak Brønsted sites (hb) and physisorbed (ph) pyridine appear at 1598 cm^{-1} (hb 8a mode), 1588 cm^{-1} (shoulder, ph 8a mode), 1581 cm^{-1} (hb, ph 8b mode), 1485 cm^{-1} (shoulder, hb, ph 19a mode), 1446 cm^{-1} (hb 19b mode), and 1439 cm^{-1} (shoulder, ph 19b mode) [42,44]. In contrast to pyridine, the adsorbed collidine (Fig. 3c) does not show a characteristic band for a protonated species, which suggests that most strong acid sites are located inside the zeolite structure. The main features can be assigned in the following way: 1617 cm^{-1} (hb 8a mode), 1611 cm^{-1} (shoulder, ph 8a mode), 1572 cm^{-1} (hb, ph 8b mode), 1450 cm^{-1} (broad and multicomponent, hb, ph, 19a and 19b modes), 1377 cm^{-1} (CH_3 groups bending vibrations) [43,48].

Fig. 4 shows the OH-stretch region of the 100 nm and 300 nm series of ZSM-5 materials, and desilicated ZSM-5 after outgassing at 623 and 773 K. The gray and black curves correspond to the outgassing temperatures at 623 and 773 K, respectively. The important observations in the complete set of spectra are the following:

i. The intensities for the hydroxyl species are significantly different in the series especially in case of samples activated at 773 K; in particular, NZ-100/83, NZ-100/150, NZ-300/120, and NZ-300/91 show an overall lower intensity with respect to each other.

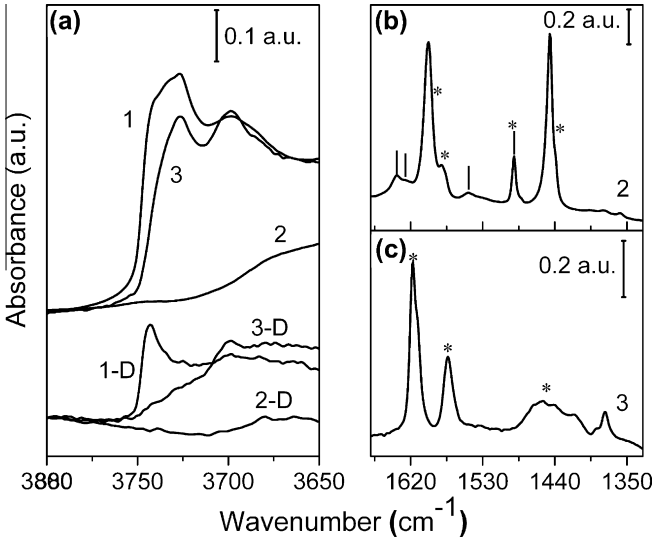

Fig. 3. FTIR spectra of pyridine and collidine adsorption on NZ-100/152 and NZ-300/120-D samples. (Part a) shows the weak acidic hydroxyl group range (3800–3650 cm^{-1}) of the NZ-100/152 and DZ-300/120 samples before adsorption (curves 1 and 1-D, respectively), after interaction with pyridine (curves 2 and 2-D, respectively) and collidine (curves 3 and 3-D, respectively) vapor pressure. (Parts b and c) show the irreversible portion of pyridine and collidine interacting with NZ-100/152. Peaks marked with (∗) symbol are assigned to physisorbed species, while the ones marked with (|) symbol are assigned to protonated species. (a.u.) = Absorbance units.

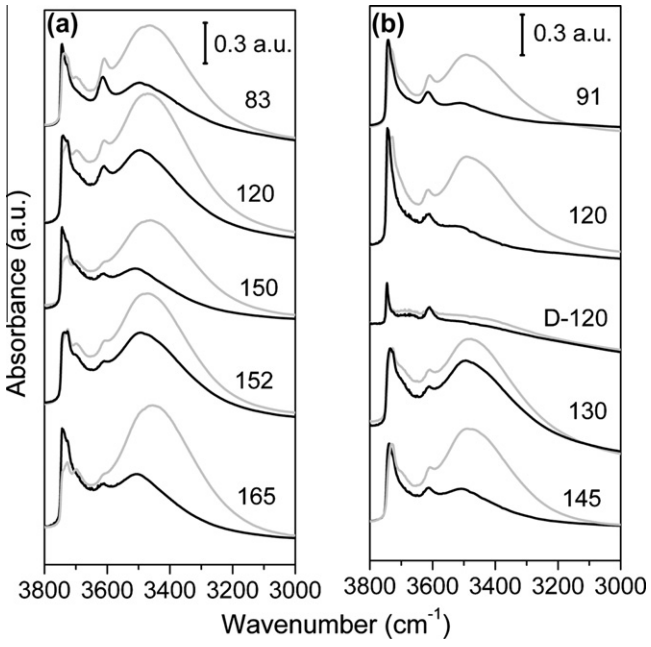

Fig. 4. FTIR spectra in the OH-stretch region (3800–3000 cm^{-1}) of the two ZSM-5 series after activation at 623 K (gray curves) and 773 K (black curves). NZ-100 series, 100 nm particle size (a) and NZ-300 series, 300 nm particle size (b). (a.u.) = Absorbance units.

ii. The increasing Si/Al ratio along the series is reflected in the decreasing intensity of the component at 3610 cm^{-1}, consistent with a decrease in the number of Brønsted acid sites in the materials.
iii. Even after a prolonged outgassing at 773 K, the intensity of the triplet at 3745, 3735, and 3726 cm^{-1} is hardly affected, indicating that these isolated silanol groups are quite stable. The decrease in intensity at 3700 cm^{-1} and at 3500 cm^{-1} upon outgassing at 773 K indicates a lower stability for the silanol nests and some of the isolated silanol groups.

To study the acid strength of the different hydroxyl groups, all samples activated at 623 and at 773 K were probed by CO adsorption at 100 K. The spectra for all samples considered in Table 1 are reported in the Supporting information (Figs. S1 and S2). As a representative example, Fig. 5 shows a complete set of spectra for increasing CO coverages on the NZ-100/152 catalyst. Parts a and b refer to the sample outgassed at 623 K; parts c and d show the data after outgassing at 773 K. The red curves indicate the spectrum of the sample before CO adsorption, and the blue curves correspond to the spectrum of the sample at the highest CO coverage; the spectra for intermediate CO coverages are depicted in gray.

Adsorption of CO at 100 K reveals the existence of different types of acid sites. At low CO coverage, the first band eroded is the one due to the strong Brønsted acid sites at 3610 cm^{-1}, which is shifted to 3302 cm^{-1}, indicating that the Brønsted acid sites are the most acidic sites in the zeolite. Upon increasing the CO pressure, first the band at 3700 cm^{-1} shifts to 3576 cm^{-1}, and the intensity decreases. Then, the intensity of the band at 3726 cm^{-1} decreases, followed by the bands at 3745 and 3735 cm^{-1}, and a single broad and intense band at 3639 cm^{-1} appears. This indicates a very similar but slightly higher acidity of the internal silanol groups (3726 cm^{-1}) compared with the external ones (3745 cm^{-1}). Finally, at the highest CO coverage, a slight perturbation of the band due to H-bonded silanol nests at 3500 cm^{-1}, which shifts to 3417 cm^{-1}, is observed.

The corresponding CO stretch frequencies are shown in Fig. 5b and d. At very low coverage, a band located at 2175 cm^{-1} is observed, corresponding to CO interacting with strong Brønsted sites. At higher CO coverage, an asymmetric band centered at 2160 cm^{-1} is observed which is assigned to CO interacting with the silanols

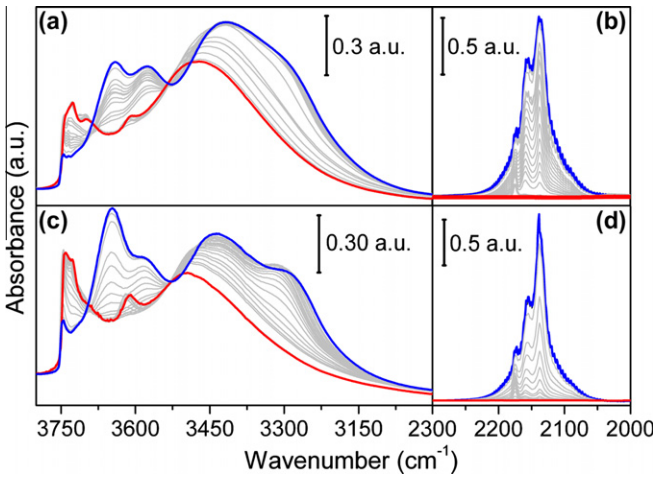

Fig. 5. FTIR spectra of CO adsorption at increasing coverage on NZ-100/152 sample activated at 623 K (Parts a and b) and 773 K (Parts c and d). (Parts a and c) report the spectra in the hydroxyl group range (3800–3000 cm^{-1}) while (Parts b and d) show the CO vibrational mode region (2300–2000 cm^{-1}), respectively. Red curves show background spectra, blue curves refer to highest CO coverage, while gray curves report intermediate adsorption steps. (a.u.) = Absorbance units.

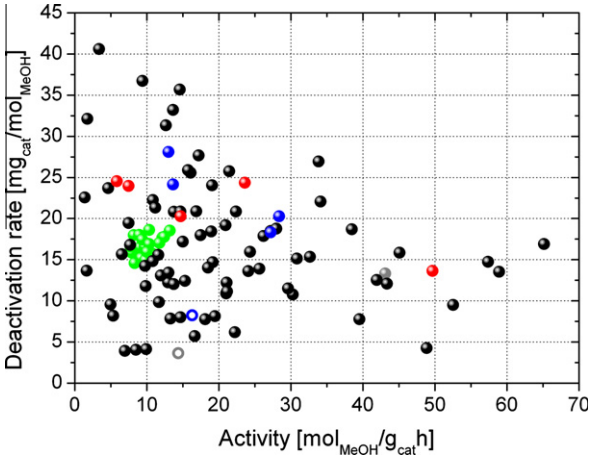

Fig. 6. Overview of deactivation rate vs. activity obtained on the over 100 tested pure ZSM-5 samples, analyzed according to a recently developed model [26]. Red and blue dots mark the 100 nm and 300 nm series, respectively. Gray symbols represent the PZ-ZSM-5. Open symbols correspond to desilicated materials. The green dots refer to the reference ZSM-5 sample used in the measurement of the deactivation.

[28,29]. We have not seen different components of this band, probably due to the very similar acidity of the silanol groups. The sharp band at 2137 cm^{-1} is assigned to a liquid-like phase condensed into the pores of the zeolite [49].

3.2. Structure–deactivation relationship

The catalytic performance of the zeolites was characterized by the activity for the conversion of methanol to hydrocarbons at 350 °C and the deactivation rate under these conditions. Fig. 6 shows an overview of the measured deactivation rates and activities of over 100 differently prepared ZSM-5 samples, including the samples that are described and discussed in this contribution. The green data points correspond to repeated measurements of the same reference sample to check the reproducibility of the deactivation measurements; the estimated accuracy of the deactivation coefficient is 18% for a single measurement [26]. As is obvious from this figure, there is no clear correlation between activity and deactivation, although we did not succeed in producing a material with both a high activity and a fast deactivation (top right corner in Fig. 6). This clearly indicates that the catalyst activity and the deactivation depend on different physical or chemical properties of the catalyst, which can be varied independently of each other.

The conclusion that activity and deactivation depend on different catalyst properties is corroborated by a comparison of the correlations of activity and deactivation with the acidity of the catalysts (Fig. 7). The activity correlates linearly with the number of strong acid sites, measured as an NH_3 adsorption capacity. The exceptions are the PZ-ZSM-5 sample and its desilicated counterpart (gray dots in Fig. 7), which has a lower activity than expected from the trend observed for the other materials. The larger particle size of this material (0.5–2 μm) probably results in a stronger diffusion limitation for the conversion of methanol, resulting in a lower effective activity. There is, however, no clear correlation with the deactivation rate. This means that the activity is determined by the catalyst acidity, but the deactivation behavior is determined by a different property, that is not correlated with the Brønsted acidity of the materials.

Following the observed correlation between the carbon formation in the isomerization of *o*-xylene and the presence of silanol groups [23], we looked for a possible relation between the

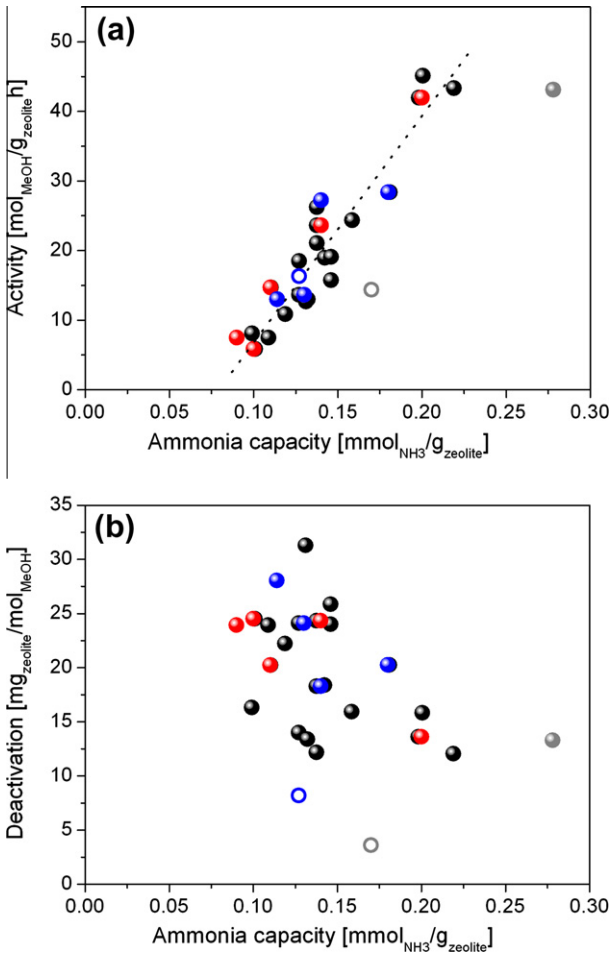

Fig. 7. Overview of the relation between acidity and activity (a) and between acidity and deactivation (b). For the two graphs, only pure ZSM-5 samples (no metal doping, etc.) have been selected. Red and blue dots mark the 100 nm and 300 nm series, respectively. Gray symbols represent the PZ-ZSM-5. Open symbols correspond to desilicated materials.

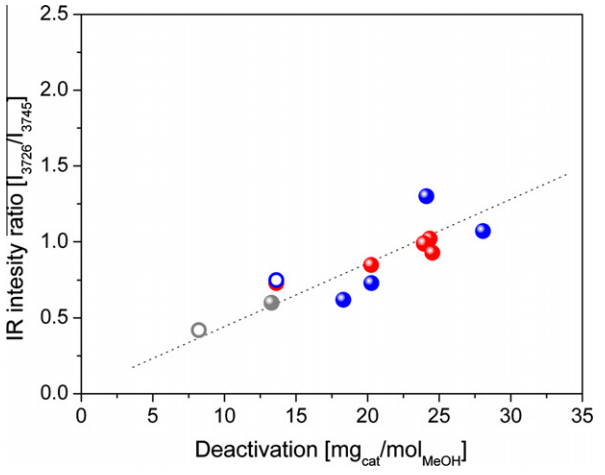

Fig. 8. Correlation between the deactivation rate and the IR intensity ratio (I_{3726}/I_{3745}) for the 100 and 300 nm series, red and blue dots, respectively. Gray symbols represent the PZ-ZSM-5. Open symbols correspond to desilicated materials. IR data from activation at 773 K have been used.

observed IR bands of the silanol groups and the deactivation rate. This seems reasonable, because aromatic compounds, such as xylenes, play an important role in the hydrocarbon pool mechanism that governs the MTH reaction over ZSM-5 [16,50–70]. Fig. 8 shows a graph of the intensity ratio of the features at 3726 cm^{-1} (an internal isolated silanol) and 3745 cm^{-1} (external silanol) (I_{3726}/I_{3745}) against the measured deactivation rate. By using intensity ratios rather than band areas, erroneous determination of background contributions and excessive data manipulation to resolve overlapping bands is avoided. As is seen, a surprisingly clear linear correlation exists between the measured deactivation rates and the ratio I_{3726}/I_{3745}, indicating that the presence of silanol groups in the zeolite affects the deactivation rate. This leads to the conclusion that the parameter determining the deactivation is related to the amount of silanol groups inside the zeolite. This parameter also fulfills the requirement that it is not dependent on the Brønsted acid site density, as also was shown in the IR of adsorbed CO, and can therefore also account for the absence of a correlation between activity or Brønsted acid site density and deactivation rate.

4. Discussion

The results show a clear correlation between the deactivation behavior and the intensities for the isolated silanol bands in the IR spectrum at 3726 and 3745 cm^{-1}, corresponding to the internal silanol groups and the silanol groups on the external surface of the zeolite, respectively. The practical consequence of this correlation is that the shape of the IR signal in the range 3700–3750 cm^{-1} reveals whether a material can be expected to have a rather stable activity or to deactivate fast.

The observed correlation between the intensity of the IR bands for the silanol groups and the deactivation rate points to a contribution of internal coke to deactivation and the importance of the internal silanol groups. The fact that the particle size and therefore the external surface sites (silanols) do not directly correlate with the deactivation is shown in Fig. 7b. This demonstrates that external coking does not play a dominant role when a significant amount of internal defects is present at the same time. The coking at the internal framework defects appears very effective compared with the coking at the external surface, and as a consequence, small amounts of coke at internal defects could contribute significantly to the deactivation. Therefore, deactivation by internal coke may explain the large differences in the amount of coke before deactivation is observed [7]. The internal silanol groups interact in some way with the coke precursors to stabilize these.

A more precise translation of the correlation between deactivation and the ratio I_{3726}/I_{3745} is that a ZSM-5 based zeolite material with a low internal silanol density or a high external surface area, or both, will show a slow deactivation in the conversion of methanol to hydrocarbons. The requirement of a high external surface area, which is equivalent to small particles, to obtain a stable catalyst is well known [71–74] and is consistent with a pore blocking mechanism for deactivation. The need of a low number of internal silanol groups has been proposed earlier [23], but at the moment it is not clear how these internal silanol groups affect the deactivation of ZSM-5 based catalyst in the conversion of methanol to hydrocarbons.

The intensity ratio I_{3726}/I_{3745} can be interpreted as the amount of internal silanol groups per m^2 external surface area. In fact, the intensity of the band at 3745 cm^{-1} has been used to estimate the external surface area of a ZSM-5 zeolite [30,75]. The result that the deactivation rate of a material is determined by the amount of internal silanol groups normalized to the external surface area is not well understood yet. Intuitively, one would expect a dependence on the amount of silanol groups normalized to the total amount or total volume of catalyst, resulting in a density of inter-

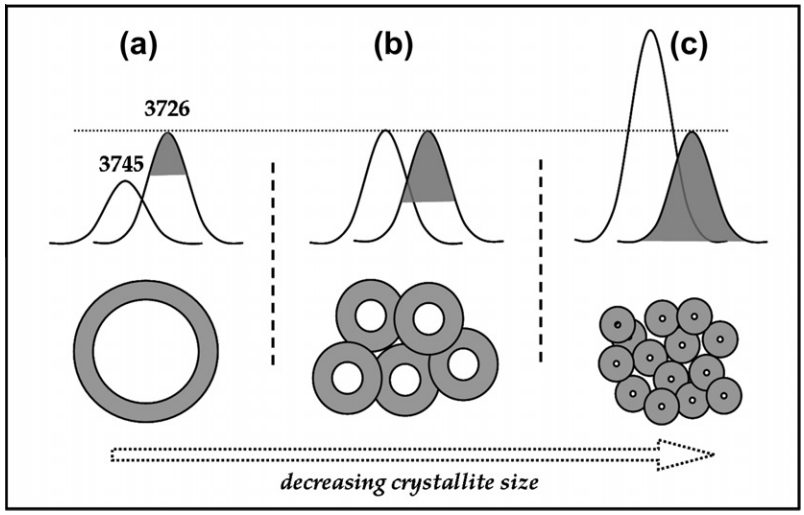

Fig. 9. Schematic drawing of the *Gedankenexperiment*, showing the measured IR intensities of internal and external silanol groups for different particle sizes, and the parts of the catalyst particles contributing to the overall activity.

nal silanol groups, similar to the Brønsted acid site density. However, the normalization to the external surface area suggests an influence of diffusion on the deactivation. Due to the microporous nature of zeolites and structural defects, diffusion of molecules of similar size as the micropores (about 5 Å), such as polymethylated benzenes, is slow. In the following, a few scenarios for the possible role of diffusion for catalyst deactivation are discussed.

In Fig. 9, a Gedankenexperiment is drawn. The three parts in the figure represent a fixed amount of a catalyst with different particle sizes and an accordingly different number of particles. It is assumed that the internal silanol groups are distributed homogeneously through the material; the density of the internal silanol groups is the same in all three cases. The intensities of the IR bands at 3745 and 3726 cm^{-1} are indicated as well. The intensity of the IR band at 3726 cm^{-1} is the same in all three cases, as the total amount of internal silanol groups is the same. The intensity of the band at 3745 cm^{-1} is proportional to the external surface area and is therefore more intense for the smaller particles.

Based on the observation that the deactivation rate is proportional to the amount of internal silanol groups, we assume that deactivation occurs by deposition of hydrocarbon fragments inside the zeolite channels. Full deactivation occurs when the accessible range of the catalyst particles is filled. For large particles (panel a), this corresponds to a shell at the outer surface of the particles; for smaller particles, this can be the entire volume of the particles (shaded areas in Fig. 9).

This means that a zeolite with a high ratio for I_{3726}/I_{3745} (panel a, large particles) is expected to deactivate fast, which agrees with the observed correlation. The intensity ratio I_{3726}/I_{3745} then reflects the abundance of the effective amount of internal defects causing deactivation. This scenario resembles that of pore mouth blocking and is also consistent with the observation that coke formation takes place at the edges of the zeolite-crystallites [76]. However, the correlation also predicts that a zeolite with a higher density of internal zeolite groups deactivates faster: If the presence of the silanol groups results in a slower diffusion, the accessible ranges become smaller and a faster deactivation results.

Although the concept of an accessible range in the catalyst particles as explained above agrees qualitatively with the observed correlation between the silanol density and deactivation, the catalytic activity for the 100 and 300 nm particles is not affected by the particle size, pointing to a fast diffusion in these materials. The measured activities for the 100 nm and 300 nm series of zeolites depend on the acidity of the materials in the same way (see Fig. 7a). In the case of a diffusion limited reaction, one would expect a lower activity per acid site for the 300 nm particles, since a smaller fraction of the acid sites is actually used in the reaction, and a lower slope in Fig. 7a is expected for the 300 nm particles. For the larger ZSM-5 particles (0.5–2 μm), the lower slope is actually observed.

This inconsistency could be resolved by realizing that the catalytic activity is determined by the diffusion rate of the methanol or DME, while the deactivation rate is controlled by the diffusion of some hydrocarbon products, presumably polymethylated benzenes (PMB). Since the methanol molecules are smaller in size, it is expected that they diffuse faster through the zeolite crystals. Consequently, the conversion of methanol takes place over the entire volume of the catalyst particles, and the PMB are deposited in the entire volume of the catalyst particle. Such a scenario has been proposed earlier by Chen et al., who concluded that the initial deposition of coke takes place inside the zeolite channels [77], and results in an inactive or inaccessible zone in the center of the particles, as previously proposed by Beyne et al. [78]. The accumulation of PMB in the particles then depends on the activity and the rate at which the PMB is transferred from the catalyst particle to the gas phase. This transfer is controlled by the diffusion coefficient and the outer surface area of the particle. In large particles, the PMB formed inside in the center of the particles (white areas in Fig. 9) do not reach the gas phase, and hence a fast deactivation occurs. For smaller particles, the PMB accumulation in the catalyst particles is slower, because the transfer to the gas phase is more efficient as a consequence of both a larger total surface area and the shorter distance to be covered by diffusion. If we again assume that the diffusion becomes slower with an increasing internal silanol density, we find that particles with a high silanol density or low external surface area are expected to deactivate fast, which agrees qualitatively with the observed correlation in Fig. 8.

The internal silanol groups seem to play an important role for the deactivation of the ZSM-5 catalyst in the conversion of methanol to hydrocarbons. It is obvious that silanol groups can be formed at the outer boundaries of a crystal, as the silanol groups here constitute a natural surface termination of the zeolite crystal structure. In contrast, the internal silanol groups necessarily represent defects in the bulk crystals of the zeolite, since a perfect zeolite crystal does not contain any silanol groups. Calculations on defective silicalite structures [31–33] show that internal silanol groups are

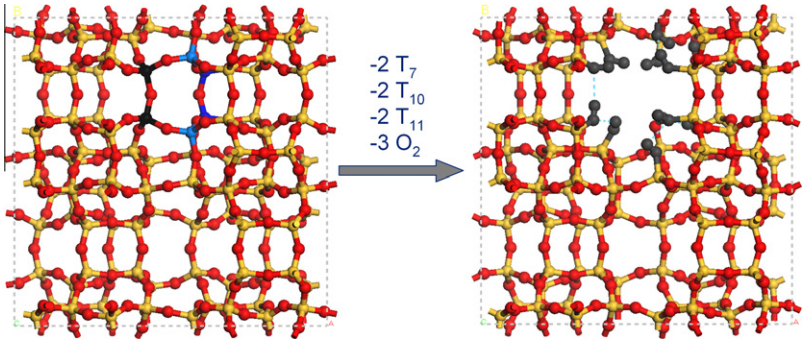

Fig. 10. MFI-unit cells oriented along *Z* axis. Left: 6T sites, forming a 6-member ring, have been selected to create a local defect (T7 black, T11 light blue, and T10 dark blue). Right: Internal defect generated upon removal of 6T sites and 6 oxygen and formation of 12 OH groups.

typically arranged in chains or rings, while external silanols are simply described as isolated species and to a minor degree as vicinal. It was shown that the acid strength of the terminal silanol groups directly correlates with the number of silanol groups in the chain [33]. In view of these results, the highest frequency component at 3745 cm^{-1} can be assigned to free silanol groups, associated with isolated species, which pre-dominantly occurs at the external surface of the zeolite crystals. The features at 3735, 3726, and 3700 cm^{-1} are related to silanol groups in short and long chain terminal positions. This is consistent with the slightly stronger interaction of these silanol groups with CO (Fig. 4), indicating a stronger acidity. These are mainly located inside the zeolite crystals, as shown by the pyridine and collidine adsorption experiments (Fig. 3) [27,28,31,33].

A ring-like arrangement of silanol groups is shown in Fig. 10. Left panel of this figure displays a perfect MFI-unit cell, in which 6 T sites forming a 6-member ring are marked (T7 black, T11 dark blue, and T10 light blue). Removal of the marked T-atoms in panel a together with six oxygen atoms results in the defective structure shown in right panel. The dangling bonds are saturated with 12 OH groups, resulting in the ring-like arrangement of the silanol groups. The cyan dotted lines illustrate the formation of H-bonds between these silanol groups.

A defect structure that produces chains of weakly interacting internal silanol groups is an intergrowth structure (twin planes) within the zeolite particles. In fact, the presence of intergrowth structures is common in ZSM-5 crystals [79–82], and they arise in the planes where two crystalline domains that are displaced or rotated with respect to each other meet. In these planes, the intact bridging ≡Si—O—Si≡ bonds alternate with dangling silanol groups, resulting in a weak interaction between them. This structure is shown in Fig. 11. The silanols at the domain boundaries are inside the zeolite particles and therefore not accessible for a molecule like 2,4,6-collidine. Further, it is likely that at such crystal intergrowth boundaries the diffusion for molecules like PMB's is hindered. Müller et al. [83] found that the diffusion coefficients of toluene in ZSM-5 samples with intergrowth structure are up to 3 orders of magnitude lower than with single crystals. Mores et al. [76] measured fluorescence intensity profiles of large H-ZSM-5 crystals, containing intergrowth defects, during the methanol to olefins (MTO) reaction and observed different penetration rates for differently methylated benzenes. The fact that the particle sizes from SEM and crystalline domain sizes from XRD for the 100 nm series indicated that monocrystalline particles do not strictly exclude the possible presence of twin planes or intergrowth structures. A twin plane does not automatically affect the width of the XRD peaks, as the lattice distance perpendicular to the twin plane does not necessarily change. Therefore, twin planes can exist, even though the XRD size and SEM particle size are the same.

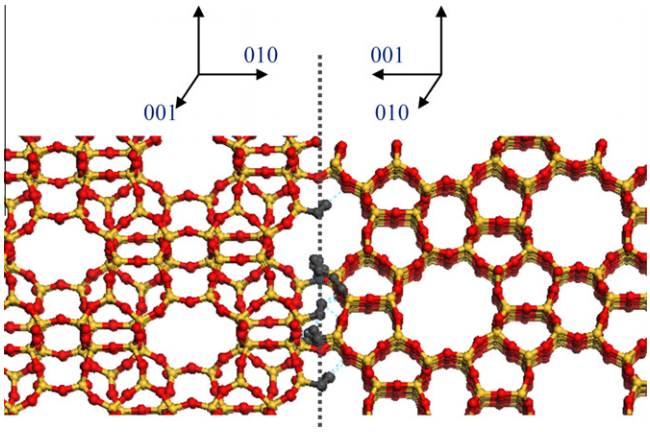

Fig. 11. Structural drawing of a hypothetic intergrowth plane, constructed by interconnection of two ZSM-5 crystals that are rotated 90° along the (1 0 0) axis with respect to each other. This is an example of how chains of weakly interacting internal silanol groups can be created.

These results agree well with the discussion above that the presence of internal silanol groups results in a slower diffusion of the PMB, which finally results in a faster deactivation. This then suggests that the silanol groups formed at these intergrowth planes are the internal silanol groups controlling the catalyst deactivation.

5. Conclusions

A large number of H-ZSM-5 based catalysts have been tested in the conversion of methanol to hydrocarbons and were characterized by infrared spectroscopy, including using CO, pyridine, and 2,4,6-collidine as probe molecules. Infrared spectroscopy reveals the presence of different types of OH groups in the range 3750–3400 cm^{-1}, namely the Brønsted acid sites and silanol groups in different local environments. By adsorption of pyridine and 2,4,6,-collidine, it is established that the infrared absorption band at 3745 cm^{-1} is associated with isolated silanol groups at the external surface of the zeolite. The bands at 3726, and 3700 cm^{-1} can be assigned to silanol groups inside the zeolite.

The activity of the materials depends on the acid site density, which can be determined by ammonia desorption. However, there

is no clear correlation between the deactivation rate and the activity of the materials, indicating that deactivation is governed by another parameter that does not depend on the acid site density. It was found that the deactivation rate correlates with the intensity ratio of the infrared absorption bands at 3726 and 3745 cm^{-1} (I_{3726}/I_{3745}), corresponding to internal and external silanol groups. This indicates that the presence of silanol groups, which are present internally in framework defects, is crucial for the deactivation of the ZSM-5 materials.

The ratio I_{3726}/I_{3745} can be interpreted as the silanol density inside the zeolite materials divided by the outer surface area. Consequently, materials with a low internal silanol density or a large external surface area (or both) are expected to show a slow deactivation in the conversion of methanol to hydrocarbons. The normalization to the outer surface area may point to an effect of the diffusion of the hydrocarbon products in the zeolite channels. In such a scenario, the silanol groups interact with the hydrocarbons to result in a slower diffusion, and a correspondingly faster deactivation.

In the literature of the last 25 years, the relative importance of internal vs. external coking, in particular in the case of ZSM-5 during MTH reaction, has been discussed in a controversial manner. The presented data in this contribution clearly show that apart from the commonly recognized deactivation of ZSM-5 due to coking at the external surface and the irreversible deactivation via dealumination, deactivation via coking at internal defects of MFI plays an important role. The presented results may explain many of the apparently contradicting results in the literature, where large differences in the amount of coke before deactivation were observed.

Appendix A. Supplementary material

Supplementary data associated with this article can be found, in the online version, at doi:10.1016/j.jcat.2011.03.016.

References

[1] C.D. Chang, A.J. Silvestri, J. Catal. 47 (1977) 249.
[2] C.D. Chang, W. Lang, A.J. Silvestri, J. Catal. 56 (1979) 268.
[3] C.D. Chang, Chem. Eng. Sci. 35 (1980) 619.
[4] J. Topp-Jørgensen, Studies in Surface Science and Catalysis, vol. 36, Elsevier Science Publishers B.V, Amsterdam, 1988, p. 293.
[5] F.J. Keil, Micropor. Mesopor. Mater. 29 (1999) 49.
[6] M. Stöcker, Micropor. Mesopor. Mater. 29 (1999) 3.
[7] T. Behrsing, H. Jaeger, J.V. Sanders, Appl. Catal. 54 (1989) 289.
[8] M. Guisnet, P. Magnoux, Appl. Catal. 54 (1989) 1.
[9] D.M. Bibby, R.F. Howe, G.D. McLellan, Appl. Catal. A 93 (1992) 1.
[10] M. Bjørgen, U. Olsbye, S. Kolboe, J. Catal. 215 (2003) 30.
[11] F. Bauer, H.G. Karge, Molecular Sieves – Science and Technology, vol. 5, Springer-Verlag, Berlin – Heidelberg, 2006, p. 249.
[12] M. Guisnet, P. Magnoux, Appl. Catal. A 212 (2001) 83.
[13] I.M. Dahl, S. Kolboe, Catal. Lett. 20 (1993) 329.
[14] I.M. Dahl, S. Kolboe, J. Catal. 149 (1994) 458.
[15] I.M. Dahl, S. Kolboe, J. Catal. 161 (1996) 304.
[16] Z. Yan, D. Ma, J. Zhuang, X. Liu, X. Liu, X. Han, X. Bao, Phys. Chem. Chem. Phys. 4 (2002) 4602.
[17] K. Wandelt, Surf. Sci. 251–252 (1991) 387.
[18] J. Maier, Angew. Chem. Int. Ed. 32 (1993) 528.
[19] N. Lopez, T.V.W. Janssens, B.S. Clausen, Y. Xu, M. Mavrikakis, T. Bligaard, J.K. Nørskov, J. Catal. 223 (2004) 232.
[20] G.P. Heitmann, G. Dahlhoff, W.F. Holderich, J. Catal. 186 (1999) 12.
[21] C. Flego, L. Dalloro, Micropor. Mesopor. Mater. 60 (2003) 263.
[22] B. Bonelli, L. Forni, A. Aloise, J.B. Nagy, G. Fornasari, E. Garrone, A. Gedeon, G. Giordano, F. Trifirò, Micropor. Mesopor. Mater. 101 (2007) 153.
[23] F. Thibault-Starzyk, A. Vimont, J.P. Gilson, Catal. Today 70 (2001) 227.
[24] H.G. Karge, W. Nießen, H. Bludau, Appl. Catal. A 146 (1996) 339.
[25] F. Bauer, E. Geidel, W. Geyer, C. Peuker, Micropor. Mesopor. Mater. 29 (1999) 109.
[26] T.V.W. Janssens, J. Catal. 264 (2009) 130.
[27] N.Y. Topsøe, K. Pedersen, E.G. Derouane, J. Catal. 70 (1981) 41.
[28] A. Zecchina, S. Bordiga, G. Spoto, L. Marchese, G. Petrini, G. Leofanti, M. Radovan, J. Phys. Chem. 96 (1992) 4991.
[29] A. Zecchina, S. Bordiga, G. Spoto, D. Scarano, G. Petrini, G. Leofanti, M. Padovan C. O. n, J. Chem. Soc. Faraday Trans. 88 (1992) 2959.
[30] S.B. Pu, T. Inui, Zeolites 19 (1997) 452.
[31] S. Bordiga, I. Roggero, P. Ugliengo, A. Zecchina, V. Bolis, G. Artioli, R. Buzzoni, G. Marra, F. Rivetti, G. Spanò, C. Lamberti, J. Chem. Soc. Dalton Trans. (2000) 3921.
[32] S. Bordiga, P. Ugliengo, A. Damin, C. Lamberti, G. Spoto, A. Zecchina, G. Spanò, R. Buzzoni, L. Dalloro, F. Rivetti, Top. Catal. 15 (2001) 43.
[33] V. Bolis, C. Busco, S. Bordiga, P. Ugliengo, C. Lamberti, A. Zecchina, Appl. Surf. Sci. 196 (2002) 56.
[34] R.M. Dessau, E.W. Valyocsik, N.H. Goeke, Zeolites 12 (1992) 776.
[35] M. Ogura, S.Y. Shinomiya, J. Tateno, Y. Nara, E. Kikuchi, M. Matsukata, Chem. Lett. (2000) 882.
[36] M. Ogura, S.y. Shinomiya, J. Tateno, Y. Nara, M. Nomura, E. Kikuchi, M. Matsukata, Appl. Catal. A 219 (2001) 33.
[37] J.C. Groen, J.A. Moulijn, J. Pérez-Ramírez, Micropor. Mesopor. Mater. 87 (2005) 153.
[38] J.C. Groen, J.A. Moulijn, J. Pérez-Ramírez, J. Mater. Chem. 16 (2006) 2121.
[39] M. Kustova, M.S. Holm, C.H. Christensen, Y.H. Pan, P. Beato, T.V.W. Janssens, F. Joensen, J. Nerlov, in: Studies in Surface Science and Catalysis Zeolites and Related Materials: Trends, Targets and Challenges, Proceedings of the 4th International FEZA Conference, vol. 174, Elsevier B.V., 2008, p. 117.
[40] B.J. Schoeman, J. Sterte, J.E. Otterstedt, Zeolites 14 (1994) 110.
[41] B.J. Schoeman, Micropor. Mater. 9 (1997) 267.
[42] R. Buzzoni, S. Bordiga, G. Ricchiardi, C. Lamberti, A. Zecchina, G. Bellussi, Langmuir 12 (1996) 930.
[43] J.Z. Flejszar-Olszewska, A.S. Muszynski, J.P. Hawranek, J. Mol. Struct. 404 (1997) 247.
[44] F. Bonino, A. Damin, S. Bordiga, C. Lamberti, A. Zecchina, Langmuir 19 (2003) 2155.
[45] C. Morterra, G. Meligrana, G. Cerrato, V. Solinas, E. Rombi, M.F. Sini, Langmuir 19 (2003) 5344.
[46] M.S. Holm, S. Svelle, F. Joensen, P. Beato, C.H. Christensen, S. Bordiga, M. Bjørgen, Appl. Catal. A 356 (2009) 23.
[47] F. Thibault-Starzyk, I. Stan, S. Abelló, A. Bonilla, K. Thomas, C. Fernandez, J.P. Gilson, J. Pérez-Ramírez, J. Catal. 264 (2009) 11.
[48] C. Morterra, G. Cerrato, G. Meligrana, Langmuir 17 (2001) 7053.
[49] M. Bjørgen, S. Svelle, F. Joensen, J. Nerlov, S. Kolboe, F. Bonino, L. Palumbo, S. Bordiga, U. Olsbye, J. Catal. 249 (2007) 195.
[50] A. Sassi, M.A. Wildman, H.J. Ahn, P. Prasad, J.B. Nicholas, J.F. Haw, J. Phys. Chem. B 106 (2002) 2294.
[51] W. Song, D.M. Marcus, H. Fu, J.O. Ehresmann, J.F. Haw, J. Am. Chem. Soc. 124 (2002) 3844.
[52] B. Arstad, J.B. Nicholas, J.F. Haw, J. Am. Chem. Soc. 126 (2004) 2991.
[53] M. Bjørgen, U. Olsbye, S. Svelle, S. Kolboe, Catal. Lett. 93 (2004) 37.
[54] D. Lesthaeghe, V. Van Speybroeck, G.B. Marin, M. Waroquier, Angew. Chem. Int. Ed. 45 (2006) 1714.
[55] D. Lesthaeghe, B. De Sterck, V. Van Speybroeck, G.B. Marin, M. Waroquier, Angew. Chem. Int. Ed. 46 (2007) 1311.
[56] D. Lesthaeghe, V. Van Speybroeck, G.B. Marin, M. Waroquier, in: Studies in Surface Science and Catalysis – From Zeolites to Porous MOF Materials – The 40th Anniversary of International Zeolite Conference, Proceedings of the 15th International Zeolite Conference, vol. 170, Elsevier B.V., 2007, p. 1668.
[57] D. Lesthaeghe, V. Van Speybroeck, G.B. Marin, M. Waroquier, Ind. Eng. Chem. Res. 46 (2007) 8832.
[58] S. Svelle, U. Olsbye, F. Joensen, M. Bjørgen, J. Phys. Chem. C 111 (2007) 17981.
[59] Z.M. Cui, Q. Liu, S.W. Bain, M. Zhuo, W.G. Song, J. Phys. Chem. C 112 (2008) 2685.
[60] Z.M. Cui, Q. Liu, Z. Ma, S.W. Bian, W.G. Song, J. Catal. 258 (2008) 83.
[61] D. Lesthaeghe, V. Van Speybroeck, M. Waroquier, Studies in Surface Science and Catalysis, vol. 174, Elsevier B.V., 2008, p. 741.
[62] D.M. McCann, D. Lesthaeghe, P.W. Kletnieks, D.R. Guenther, M.J. Hayman, V. Van Speybroeck, M. Waroquier, J.F. Haw, Angew. Chem. Int. Ed. 47 (2008) 5179.
[63] M. Bjørgen, F. Joensen, K.P. Lillerud, U. Olsbye, S. Svelle, Catal. Today 142 (2009) 90.
[64] R. Johansson, S.L. Hruby, J. Rass-Hansen, C.H. Christensen, Catal. Lett. 127 (2009) 1.
[65] D. Lesthaeghe, A. Horré, M. Waroquier, G.B. Marin, V. Van Speybroeck, Chem. Eur. J. 15 (2009) 10803.
[66] C.M. Wang, Y.D. Wang, Z.K. Xie, Z.P. Liu, J. Phys. Chem. C 113 (2009) 4584.
[67] B. Chan, L. Radom, Can. J. Chem. 88 (2010) 866.
[68] S. Teketel, U. Olsbye, K.P. Lillerud, P. Beato, S. Svelle, Micropor. Mesopor. Mater. (2010), doi:10.1016/j.micromeso.2010.07.013.
[69] M. Vandichel, D. Lesthaeghe, J.V. Mynsbrugge, M. Waroquier, V. Van Speybroeck, J. Catal. 271 (2010) 67.
[70] C.M. Wang, Y.D. Wang, H.X. Liu, Z.K. Xie, Z.P. Liu, J. Catal. 271 (2010) 386.
[71] M. Sugimoto, H. Katsuno, K. Takatsu, N. Kawata, Zeolites 7 (1987) 503.
[72] M. Yamamura, K. Chaki, T. Wakatsuki, H. Okado, K. Fujimoto, Zeolites 14 (1994) 643.
[73] L.F. Petrik, C.T. O'Connor, S. Schwarz, Stud. Surf. Sci. Catal. 94 (1995) 517.
[74] R. Van Grieken, J.M. Escola, J. Moreno, R. Rodríguez, Appl. Catal. A 305 (2006) 176.
[75] G.V. Echevsky, A.B. Ayupov, E.A. Paukshtis, D.J. O'Rear, C.L. Kibby, Studies in Surface Science and Catalysis, vol. 139, Elsevier B.V., 2001, p. 77.
[76] D. Mores, E. Stavitski, M.H.F. Kox, J. Kornatowski, U. Olsbye, B.M. Weckhuysen, Chem. Eur. J. 14 (2008) 11320.

[77] D. Chen, H.P. Rebo, K. Moljord, A. Holmen, Chem. Eng. Sci. 51 (1996) 2687.
[78] A.O.E. Beyne, G.F. Froment, Chem. Eng. Sci. 48 (1993) 503.
[79] M.B.J. Roeffaers, R. Ameloot, M. Baruah, H. Uji-i, M. Bulut, G. De Cremer, U. Iler, P.A. Jacobs, J. Hofkens, B.F. Sels, D.E. De Vos, J. Am. Chem. Soc. 130 (2008) 5763.
[80] J. Caro, M. Noack, J. Richter-Mendau, F. Marlow, D. Petersohn, M. Griepentrog, J. Kornatowski, J. Phys. Chem. 97 (1993) 13685.
[81] L. Karwacki, E. Stavitski, M.H.F. Kox, J. Kornatowski, B.M. Weckhuysen, Studies in Surface Science and Catalysis, vol. 174, Elsevier B.V., 2008, p. 757.
[82] E. Stavitski, M.R. Drury, D.A.M. De Winter, M.H.F. Kox, B.M. Weckhuysen, Angew. Chem. Int. Ed. 47 (2008) 5637.
[83] G. Müller, T. Narbeshuber, G. Mirth, J.A. Lercher, J. Phys. Chem. 98 (1994) 7436.